AIAA JOURNAL
Vol. 44, No. 3, March 2006

Aerodynamic Interactions Between Adjacent Slender Bodies

D. Weihs,* M. Ringel,† and M. Victor‡
Technion—Israel Institute of Technology, 32000 Haifa, Israel

Most externally carried aircraft stores are basically slender bodies. These stores are usually carried underneath the wings or fuselage (itself a slender body), and in many cases multiple bodies are carried in proximity. This proximity introduces new interaction forces, both in the longitudinal and lateral directions. Wind-tunnel experiments on a pair of generic slender bodies, ellipsoids of a 6:1 slenderness ratio placed in parallel in the longitudinal direction, at various lateral spacings and axial displacement, are described. The results show that significant side and axial forces are obtained. The results are then compared to calculations based on a theoretical model applied to the interaction of pairs of such slender bodies, with very good agreement, up to the limits of the first-order model. When the bodies are positioned correctly, the axial interaction force counters all of the viscous drag on one of the bodies.

Nomenclature

D	=	doublet strength
d	=	maximal diameter of slender body
F	=	force
G	=	normalized force; see definition in Eq. (11)
L	=	nominal length of wind-tunnel models
l	=	length of general slender body
$r(x)$	=	local radius of slender body
S	=	maximal cross section of body
$S(x)$	=	local body cross-sectional area, $\pi r(x)^2$
t	=	time
U, V	=	speed in x and y directions, respectively
X, Y	=	force in x and y directions, respectively
x	=	Cartesian coordinate along long axis of body
y	=	Cartesian coordinate in plane including the long axes of both bodies
z	=	third Cartesian coordinate
η	=	distance between centroids in the y direction
μ	=	strength of secondary singularity induced by the other body
ξ	=	distance between centroids in the x direction
ρ	=	density of air
φ	=	flow potential

Subscripts

i	=	index
x	=	in x direction
y	=	in y direction
0	=	fixed system
1	=	related to first body (Fig. 2)
2	=	related to second body

Introduction

SLENDER bodies of various types are frequently placed in close lateral proximity in aerospace systems. Examples include external underwing stores such as external fuel tanks, ordnance, and sensor pods. When such bodies move in air (or water), they are subjected to aerodynamic forces resulting from theproximity of neighbor bodies. In a recent theoretical study[1] on dolphin mother–calf interactions, the presence of a neighboring body was shown to result in side forces of the order of the drag force on each body (known as Bernoulli attraction), and by suitable spacing in the longitudinal direction, the rear body was shown to have much lower drag. Marine mammals such as dolphins use this phenomenon to assist young and weak members of the group by drafting.[1] The aforementioned study was based on slender-body theory,[2,3] but no experimental data for the actual forces were found, except for aerial observations of positioning of dolphins in groups. These observations closely followed the predictions for optimal positioning of the calves for assistance by the adult, but no quantitative force measurements on the animals could be performed.

In the present paper, an experimental wind-tunnel study of the forces induced on identical neighboring slender bodies of revolution is performed and the results compared to the predictions of slender-body theory. It is shown that the measured forces are in general agreement with the theory and that proper relative placing of bodies results in dramatic force changes, even resulting in thrust on one of the bodies, if placed in the right position.

Theoretical Background

A brief summary of slender-body theory[2] and its application to the two-body problem is presented here. We start by defining a slender body as having an elongate shape, that is, $d/l \ll 1$. As a result, flow characteristics do not change rapidly in the longitudinal x direction. The flowfield around it can, thus, be assumed to be a series of two-dimensional flowfields around each cross section[2] only slightly differing from each other.

To simplify matters, we only look at bodies of revolution, that is, bodies, whose cross-sectional area is $S = \pi r^2$, where $r(x)$ is the local cross section radius (Fig. 1). For motion in the direction of the longitudinal axis, the only change in the flowfield is due to changes in the local radius and the flow around the whole body can be described by a the flow around a row of doublet-type singularities at the axis.[4] As a result, a single symmetric closed body such as our spheroid will experience zero net force (the D'Alembert paradox) in inviscid flow. The drag force in this case is purely of viscous origin and not included in this type of model. However, when two bodies are in proximity, the flow asymmetries caused by the presence of the neighboring body result in net forces on each of them.

The present analysis of two adjacent slender bodies closely follows the work of Tuck and Newman[3] and Wang.[5] We define Cartesian coordinate systems attached to the centroids of both bodies (Fig. 2). These coordinate systems are moving at speed U in the x direction. It is useful to relate both to a fixed coordinate system

Received 18 July 2005; revision received 31 October 2005; accepted for publication 1 November 2005.

*Distinguished Professor, Faculty of Aerospace Engineering.
†Chief Engineer, Wind Tunnel Laboratory, Faculty of Aerospace Engineering.
‡Engineer, Wind Tunnel Laboratory, Faculty of Aerospace Engineering.

Fig. 1 Slender-body models in wind tunnel.

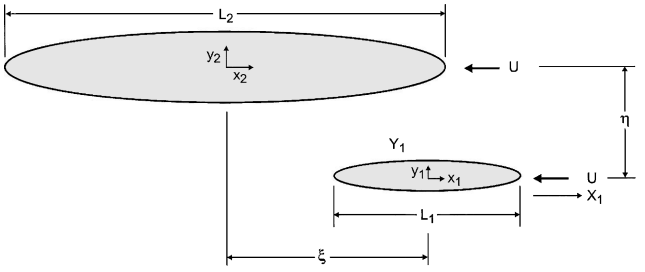

Fig. 2 Coordinate system.

so that

$$x_0 = x_1 + Ut = x_2 + Ut - \xi, \qquad y_0 = y_1 = y_2 - \eta$$
$$z_0 = z_1 = z_2 \tag{1}$$

where ξ is the stagger between the bodies.

Potential incompressible flow is described by the linear Laplace equation $\nabla^2\varphi = 0$, so that solutions can be superposed. As already mentioned, the flowfield around circular cross sections is described by uniform flow around a doublet of suitable strength so that each of the bodies when immersed in a uniform stream of speed U is described by a row of doublets of strength D_i, where S_i is the cross-sectional area,

$$D_i(x_i) = -(1/2\pi)S_i(x_i)U_i, \qquad i = 1, 2 \tag{2}$$

The potential of the flow can now be written as a sum of the potentials of flow around each body

$$\varphi(x_1, y_1) = -Ux_1 + \varphi_1(x_1, y_1) + \varphi_2(x_2, y_2) \tag{3}$$

Substituting Eq. (2) into Eq. (3) and applying the coordinate system of Fig. 3, we can write the potential for the second body as

$$\varphi_2(x_2, y_2, z_2, \xi) = -\frac{U}{2\pi}\int_{L_2} \frac{S_2(x_2)(x - x_2 + \xi)\,\mathrm{d}x}{\left[(x - x_2 + \xi)^2 + (y - \eta)^2 + z^2\right]^{\frac{3}{2}}} \tag{4}$$

We write out only the expression for the second body, identified by indices 2, to save space, because the first body is described by a similar expression. We chose body 2 because both ξ and η are zero for body 1.

We obtain the velocity at each point due to the second body by taking the suitable derivative of the potential. Specifically, the velocity components on the axis of the first body are

$$u(x_1, \xi) = \frac{\partial\varphi_2}{\partial x}(x_1, 0, 0, \xi) = \frac{U}{2\pi}\int_{L_2} \frac{S_2'(x_2)(x - x_2 - \xi)\,\mathrm{d}x_2}{\left[(x - x_2 - \xi)^2 + \eta^2\right]^{\frac{3}{2}}} \tag{5}$$

$$v(x_1, \xi) = \frac{\partial\varphi_2}{\partial y}(x_1, 0, 0, \xi) = \frac{U\eta}{2\pi}\int_{L_2} \frac{S_2'(x_2)\,\mathrm{d}x_2}{\left[(x - x_2 - \xi)^2 + \eta^2\right]^{\frac{3}{2}}} \tag{6}$$

These velocities induce additional singularities on the axis of the first body, which can be written, again assuming slender bodies, as

$$\mu_{1x}(x_1, \xi) = -(1/2\pi)S_1(x_1)U(x_1, \xi)$$
$$\mu_{1y}(x_1, \xi) = -(1/2\pi)S_1(x_1)V(x_1, \xi)$$

respectively. These singularities enable calculation of the forces on the first body, resulting from the interaction, as already mentioned. These are, to leading order,

$$F_x(\xi) = -\rho U\int S_1(x_1)\frac{\partial}{\partial\xi}U\,\mathrm{d}x_1$$
$$F_y(\xi) = -2\rho U\int S_1(x_1)\frac{\partial}{\partial\xi}V\,\mathrm{d}x_1 \tag{7}$$

Next, we integrate by parts and apply the fact that the body tips are of zero diameter and have a continuous, single-valued derivative, that is, no sharp edges or finite area,

$$X = F_x = \frac{\rho U^2}{4\pi}\int_{L_1} S_1'(x_1)\int_{L_2} \frac{S_2'(x_2)(x_2 - x_1 - \xi)\,\mathrm{d}x_2}{\left[(x_2 - x_1 - \xi)^2 + \eta^2\right]^{\frac{3}{2}}}\,\mathrm{d}x_1 \tag{8}$$

$$Y = F_y = \frac{\rho U^2\eta}{2\pi}\int_{L_1} S_1'(x_1)\int_{L_2} \frac{S_2'(x_2)\,\mathrm{d}x_2}{\left[(x_2 - x_1 - \xi)^2 + \eta^2\right]^{\frac{3}{2}}}\,\mathrm{d}x_1 \tag{9}$$

for the longitudinal and lateral forces on the first body due to the existence of the second.

To apply the general equations (8) and (9), one now needs a specific body shape. We take this to be a spheroid, with area distribution of

$$S_i(x_i) = d_i\left[1 - 4(x_i/L_i)^2\right] \tag{10}$$

where d_i is maximum girth of each at the equator. Figure 3 (adapted from Ref. 1) shows how the forces change as the relative longitudinal (fore–aft) positions of the two bodies is varied, for cases of equal sized bodies, or different sized bodies. The ordinate reads G_x and G_y [Eqs. (11a) and (11b)].

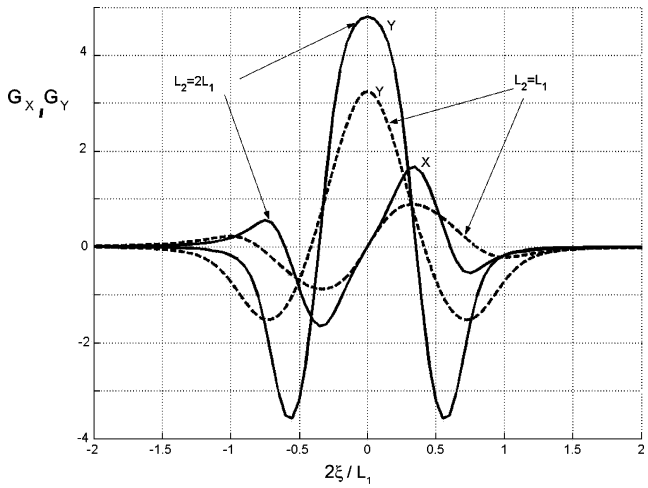

Fig. 3 Normalized lateral *Y* and longitudinal *X* forces vs relative positions of two bodies: ——, length ratio 2:1 and – – –, equal-sized bodies; all curves calculated for $\eta/L_1 = 0.25$.

Wind-Tunnel Experiments

Spheroids of 6:1 slenderness ratio and 270-mm nominal length were manufactured of stainless steel 303 and aluminum Al 2024. The rear of each spheroid was hollowed out and a sting holder of diameter 16 mm was installed within a hollow of 24-mm diameter. The models were tested in the Technion Wind Tunnel Laboratory Tunnel 1 (Fig. 1). The tunnel has a 600 × 800 mm cross section, so that the blockage for both models was less than 0.6% at zero angle of attack (at which the relevant measurements were taken), and less than 2% for angles of up to 30 deg. Forces and moments were measured by means of six-degree-of-freedom strain gauge sting balances, with a sensitivity of 3.3 μV/g for side force and 2.9 μV/g for axial force.

Two spheroids were introduced into the tunnel (Fig. 1) with parallel longitudinal axes and different ξ and η. (See Fig. 2 for definitions.) The tunnel was run at 75-m/s nominal speed, and both models were moved together through a range of angles of attack to determine the aerodynamic zero angle, defined as the geometric angle at which the drag forces were minimal.

The experiments were conducted with two spheroids of equal size, of 270-mm nominal length and 249-mm actual length. The difference is due to the sting holder in the model. The slenderness ratio is not reduced because the balance rod continues the body.

Results

Typical raw data are shown in Fig. 4, in which two equal-sized spheroids were placed so that $\xi = 0$ while varying the lateral distance η/L between centerlines. Each run, shown as a set of points forming a curve, was performed with the two spheroids being swept through a range of angles of attack. Each curve describes the lateral force Y acting on the right-hand ellipsoid for a different η/L, whereas each point is at a different time during the sweep, that is, different angle of attack. The absolute lateral distance (in millimeters) between the farthest points on the bodies in the center of mass planes is DY. The distance between centerlines is, thus, $DY - 45$ mm. The nominal length of the ellipsoids is $L = 270$ mm, that is, the top curve × is for a value of $\eta/L = 61.8/270 = 0.229$. We see that the aerodynamic zero angle of attack is about 2 deg below the nominal wind-tunnel axis horizon. This is a result of the weight of the models and the sting and balance structure. This aerodynamic zero angle was found

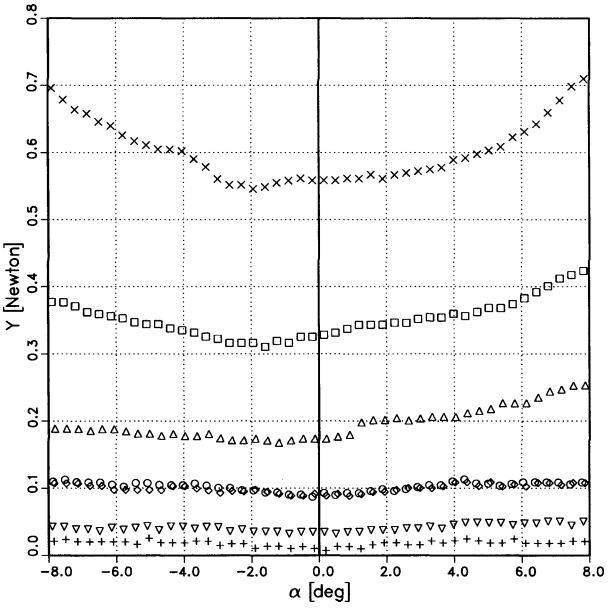

Fig. 4 Raw experimental data, side force (newtons), for 64620N ellipsoid 1:6, twin, $M = 0.22$, various lateral distances vs angle of attack: ×, 14343 balance, $DY = 106.8$ mm; □, 14341 balance, $DY = 122.8$ mm; △, 14340 balance, $DY = 144$ mm; ◇, 14352 balance, $DY = 163$ mm; ○, 14353 balance, $DY = 181$ mm; ▽, 14354 balance, $DY = 209$ mm; and +, 14355 balance, $DY = 242.5$ mm.

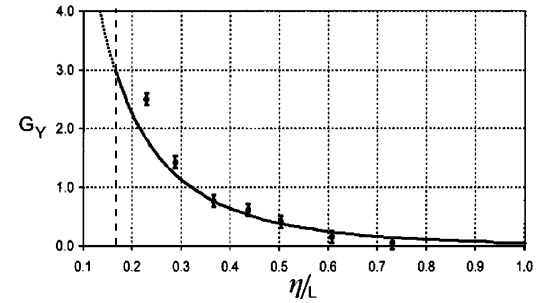

Fig. 5 Nondimensional side force vs lateral separation: ——, theory; ●, experimental data; and – – –, $\eta/L = 0.167$, closest approach physically possible (touching bodies).

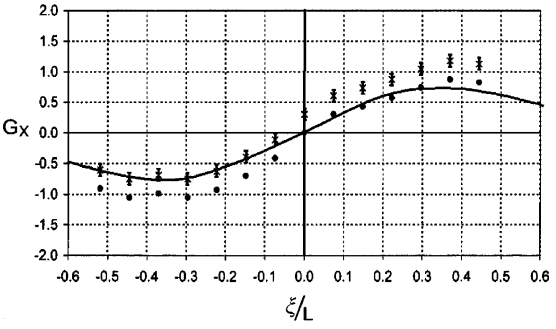

Fig. 6 Nondimensional forward force vs longitudinal displacement of the two bodies: ——, theory; ×, actual measurements; and ●, potential force (after subtracting viscous drag).

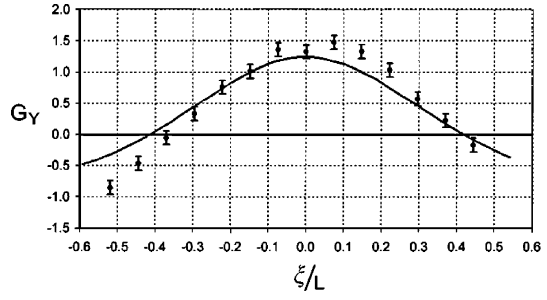

Fig. 7 Nondimensional side force vs longitudinal displacement of the two bodies: ——, theoretical prediction.

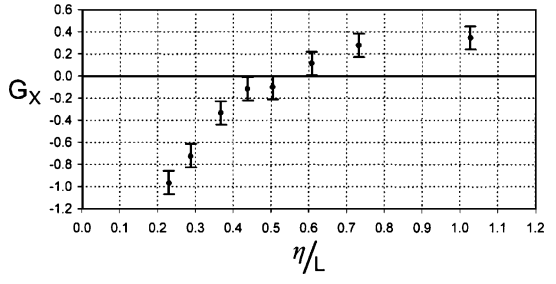

Fig. 8 Nondimensional forward force vs lateral spacing of bodies placed for maximal forward force: ——, zero force (i.e., interaction force cancels viscous drag on lagging body).

for each run, and the value of forces measured at this angle was used for Figs. 5–8. Last, the speed appears as the Mach number (0.22 for all runs). We further define a nondimensional coefficient G_Y, defined as the force divided by the dynamic pressure and the maximal cross-sectional area,

$$G_Y = (Y/\rho U^2)(L^2/S^2) \tag{11a}$$

and in similar fashion, the axial (drag) force coefficient is

$$G_X = (X/\rho U^2)(L^2/S^2) \tag{11b}$$

so that when $G_i = 1$, $i = Y, X$, in the present case the actual force is 0.244 N.

Figure 5 shows the change of maximal side force coefficient G_Y, for two equal cylinders with $\xi = 0$, as a function of lateral distance η/L between centerlines. As the results show, the theoretical calculation predicts the trend of the results, but underestimates the experimental values (circles with error bars, in Fig. 5) for the cases of smaller η/L. This is to be expected because as the calculation is based on the first-order potential model of the preceding section. As the bodies are placed closer to each other, the assumptions of the first-order model become less accurate so that such discrepancies are to be expected. The accuracy of this slender-body theory is defined by the slenderness ratio, that is, it becomes important when the distances are much less than the body length. At these lateral spacings, the viscous boundary layer reduces the effective distance between the bodies, this being most pronounced at the center of the bodies. A rough estimate of boundary-layer thickness is about 1% of the longitudinal distance from the body nose, that is, at 135-mm distance this would be 1.35 mm. At the smallest value of η/L tested, the distance between closest points on the two bodies is about 17 mm, so that viscous effects also become important.

Figure 6 shows the change in forward force as the relative position of the two bodies changes in the longitudinal direction. In Fig. 6, $\eta = 77.8$ and $\eta/L = 0.288$. The data for comparison with theory are presented in two forms. The $\times$ indicate the actual measured value, whereas the circles are obtained by subtracting the viscous drag, as measured on a single body placed at the tunnel center ($G_X = 0.39$). The remaining axial force is, thus, the effect of the neighboring body because there is no inviscid axial force on a single ellipsoid. The theoretical curve is taken from Fig. 3, for $\eta/L = 0.25$, and is added only to show the trend and the fact that, when the bodies are parallel in the lateral direction, the longitudinal force stays zero and that maximal axial forces are obtained at $\xi/L = 0.35$ roughly, again as predicted by theory. When the measured body follows the second body, a net forward force is obtained on the following body. This can be applicable for movement in formation and has been observed in dolphins.[1] One interesting point here that warrants further study is that the gain in forward force on the following body is somewhat larger than the loss (added cost) to the leading body.

Figure 7 shows the change in side force experienced by each of the bodies, as the longitudinal spacing between centroids varies from -0.6 to $+0.6$. In Fig. 7, $\eta = 77.8$ and $\eta/L = 0.288$. The full curve is the theoretical calculation adapted from Fig. 3. Here again, the experimental results clearly follow the predictions, but the actual forces are somewhat larger than the predictions when the bodies are at $\xi = 0$ and when they are highly displaced that is, viscous displacement is most significant in channeling the flow when $\xi = 0$, and in pushing sideways when highly displaced. Note that for $\xi/L = 0.35$, which is the preferred position for forward force on the follower, the side force vanishes, so that in the case of free moving bodies (such as the dolphins discussed in Ref. 1) the follower does not have to correct for lateral attractive forces toward the leader.

Figure 8 shows the change of forward force on the rear body as the lateral distance η/L is varied, for a value of $\xi/L = 0.35$, at which the forward force is maximal at all lateral spacings (Fig. 3). For $\eta/L > 1$, the drag on a single body resulting from the viscous forces is retrieved. As the lateral distance shrinks, the potential interaction forces grow, so that for $\eta/L < 0.5$ the interaction forward force on the rear body, shown here, becomes larger than the viscous drag, and a net forward force is produced.

Conclusions

The experimental results of Figs. 4–8 are seen to follow very well the trends predicted by the theoretical model, for both side forces (the Bernoulli attraction) and longitudinal forces. However, the theory somewhat underpredicts the experimental results especially for small lateral distances. There are two reasons for this discrepancy.

First, the bodies are described by slender-body theory, using singularities placed on the centerline. Thus, the real lateral distance between bodies, especially in the center section, which has the largest diameter, is much smaller. For the bodies we tested (6:1 ellipsoids of nominal length 270 mm) the bodies actually touch for $\eta/L = 0.16$, so that results for given η/L are underestimated. This error becomes significant when $\eta/L < 0.3$ because the relative error grows in this region.

Second, viscous effects do not appear in the potential theory used here. This is obvious in the longitudinal force measurements, which are skewed by the addition of a constant value of viscous drag. This value was measured by running a test with only one body located along the tunnel centerline. In the scale of Figs. 4–8, this value is $G_X = 0.39$ (Fig. 8). The experimental results show that placing two slender bodies in close proximity results in significant side and longitudinal forces on both. This can be important both for the placement and the release procedure for external stores on aircraft, which are usually slender, and are located in close lateral proximity to each other, under the relatively short span of fighter aircraft.

References

[1]Weihs, D., "The Hydrodynamics of Dolphin Drafting," *Journal of Biology*, Vol. 3, No. 2, 2004, pp. 801–815.

[2]Newman, J. N., *Marine Hydrodynamics*, MIT Press, Cambridge, MA, 1977, Chap. 7.

[3]Tuck, E. O., and Newman, J. N., "Hydrodynamic Interactions Between Ships," *Proceedings of the Tenth Symposium on Naval Hydrodynamics (ACR-204)*, Office of Naval Research, Cambridge, MA, 1974, pp. 35–58.

[4]Milne-Thomson, L. M., *Theoretical Hydrodynamics*, 5th ed., Macmillan, New York, 1968, 743 pp.

[5]Wang, S., "Dynamic Effects of Ship Passage on Moored Vessels," *Journal of Waterways and Coastal Engineering*, Vol. 101, No. 3, 1975, pp. 247–258.

A. Plotkin
Associate Editor